

Full Length Article

Self-cleaning and anti-fogging hierarchical structure arrays inspired by termite wing



Chung-Jui Lai^a, You-Jie Chen^a, Mei-Xuan Wu^a, Chia-Chien Wu^b, Nien-Ting Tang^a,
Ting-Fang Hsu^a, Shin-Hua Lin^a, Hou-Feng Li^{b,*}, Hongta Yang^{a,*}

^a Department of Chemical Engineering, National Chung Hsing University, 145 Xingda Road, Taichung 40227, Taiwan

^b Department of Entomology, National Chung Hsing University, 145 Xingda Road, Taichung 40227, Taiwan

ARTICLE INFO

Keywords:

Formosan subterranean termite
Hierarchical structure arrays
Self-assembly
Superhydrophobic
Self-cleaning
Anti-fogging

ABSTRACT

Wings of the Formosan subterranean termite (*Coptotermes formosanus* Shiraki) covered with micrometer-scale hairs and nanometer-scale wax patches, allow them to greatly reduce adhesions to water droplets of various sizes. Inspired by the anti-wetting structures, we develop a colloidal lithography-based strategy integrated with a scalable self-assembly approach to engineer hierarchical conical structure arrays. The resulting structure arrays provided a water contact angle as high as 175.3° and a low contact angle hysteresis of 2.7° after surface modification. Importantly, the resulting superhydrophobic structures even feature distinguished self-cleaning and anti-fogging capabilities. The dependence of structure configuration on the anti-wetting functionalities is also investigated in this research.

1. Introduction

Fogging occurs as moist air passes over any device or equipment with a lower temperature, which is commonly found in human daily lives such as medical treatments, and industrial processes.[1,2] The moisture condensation generates countless water microdroplets with diameters larger than visible light wavelengths, which lead to light scattering and hence cause energy loss. The resulting poor optical performance gives rise to a considerable amount of safety hazards, such as driving with foggy vehicle windshields, making use of fogged medical endoscopes in surgical treatments, and so forth. In addition to that, freezing fog build-up on overhead power lines or freezing fog-induced aerodynamic stall on airplanes in some extreme environments are even more dangerous and life-threatening.[3] To eliminate the aforementioned fogging issues, a wide variety of nanostructured hydrophilic materials have been employed to modify their surface wetting behaviors.[4–7] Instead of discrete water microdroplets, the condensed moisture tends to spread and form water films on the as-fabricated superhydrophilic coatings. Owing to strong hydrogen bond interactions with water molecules, certain constructed hydrophilic materials (e.g. poly(vinyl alcohol)) can even absorb the liquidus water.[8] Although the development of superhydrophilic coating is an effective strategy in anti-fogging, dirt and pollutants are prone to adhere onto the surface, impairing its ability to

realize film-like moisture condensation.[9] Accordingly, there is an urgent demand to improve their self-cleaning properties.

Nature is the best achievable nanotechnologist. Over 400 million years of evolution, versatile natural architectures have been developed for advanced functionalities to overcome diversified survival challenges. For example, lotus (*Nelumbo nucifera*) leaves covered with waxy raspberry-shaped structures allow air to be trapped between the hierarchical structures.[10] The contact area and adhesion forces between water droplets and water-repellent lotus leaves are significantly reduced, which results in large static water contact angles above 170° and low contact angle hysteresis below 5° on leaf surfaces. The corresponding self-cleaning properties, referred to as the lotus effect, can shield lotus leaves from any debris and pathogen even being immersed in dirty water. Indeed, numerous self-cleaning micro- and nanostructures are also found on nasturtium (*Tropaeolum*), prickly pear (*Opuntia*), lady's mantle (*Alchemilla vulgaris*), and bear cicada (*Cryptotympana takasagona* Kato) wings to name a few.[11–15] Bioinspired by the living creatures, anti-wetting structures with self-cleaning properties have been created and widely utilized.[16,17] Nevertheless, it remains a challenge to design anti-wetting structures with anti-fogging functionalities.

Recently, natural micro- and nanostructures found on certain termite wing cuticle have been demonstrated to exhibit a range of stupendous

* Corresponding authors.

E-mail addresses: houfeng@nchu.edu.tw (H.-F. Li), hyang@dragon.nchu.edu.tw (H. Yang).

<https://doi.org/10.1016/j.apsusc.2023.156484>

Received 9 November 2022; Received in revised form 8 January 2023; Accepted 16 January 2023

Available online 19 January 2023

0169-4332/© 2023 Elsevier B.V. All rights reserved.

capabilities, including superhydrophobicity, self-cleaning, and anti-fogging.[18] One of the most noteworthy examples is Formosan subterranean termite (*Coptotermes formosanus* Shiraki), originated from Taiwan.[19] The termite wings are covered with non-close-packed multiscale structures, which consist of micrometer-scale hairs and nanometer-scale wax patches. The hierarchical structures restrain the penetration of water droplets with varied sizes, and therefore offer protections against wetting by any water surface that may encounter.[20] Benefiting from their incredible anti-wetting wings, alate termites migrate and initiate a colony during either rainy or foggy conditions. Dispersal flights in high humidity environments, not only prevent termites from desiccation, but also make them easier to excavate soil or wood to form an incipient nest chamber.

The purposeful design of anti-wetting/anti-fogging structures is of increasing importance and promising in a wide spectrum of novel technological applications ranging from opto-electronic devices, water collection, water/oil separation, contamination resistance, chemical shielding, drag reduction, anti-fouling coatings, to microfluidics.[21–27] Owing to the hydrophobic micro- and nanoscopic architectures on the surface, hazardous materials with extremely reduced contact areas can be picked up by spherical water droplets, and thus easily cleaned off the surface. Inspired by the impressive multifunctionality of termite wings, a number of photolithography-based fabrication technologies can be exploited to mimic the well-arranged multiscale structures.[28,29] However, the top-down methodologies suffer from high cost and high power consumption in generating nanostructures, and the artificial features are limited by low resolution. In contrast, one-pot solvothermal treatments render a low-cost and much simpler alternative to induce condensation, solidification, and crystallization of nanocrystals for creating hierarchical structures.[30,31] The difficulty in precisely manipulating the organization of nanocrystals that fully biomimic the naturally occurring structures, nevertheless, has encumbered the development of multifunctional materials. Fueled by the rapid progress of self-assembly approaches, monolayer colloidal crystals have been widely utilized as structural templates to pattern highly ordered nanostructures.[32–34] Unfortunately, traditional bottom-up methodologies can only bring about hexagonal close-packed templates, which are not preferred for engineering bioinspired structures. Besides, most self-assembly technologies are still restricted by low-throughput, and merely accessible for laboratory-scale fabrication. Furthermore, the strategy to fabricate hierarchical structure arrays through using colloidal lithography technologies has rarely been reported.

Herein, a microfabrication-compatible and scalable spin-coating technology is developed to self-assemble monolayer non-close-packed 80 nm silica colloidal crystals and monolayer non-close-packed 590 nm silica colloidal crystals onto a polymeric substrate in succession. The double-monolayer colloidal crystals can serve as reactive ion etching masks to pattern hierarchical conical structure arrays, which significantly reduce interactions with water droplets of various size scales. The surface hydrophobicity, self-cleaning, and anti-fogging abilities of the Formosan subterranean termite-inspired hierarchical structure arrays are well investigated. By adjusting the structure configuration, anti-wetting structures with a desirable anti-fogging functionality can be achieved.

2. Experimental section

Preparation of Silica Colloidal Suspensions. The reagents, including tetraethyl orthosilicate (≥ 99.0 vol%, Merck KGaA), anhydrous ethanol (200 proof, Thomas Scientific), deionized water (18.2 M Ω .cm, Milli-Q Advantage A10 Ultrapure Water Purification System), and ammonium hydroxide (28 ~ 30 wt%, Thermo Fisher Scientific), are applied to synthesize spherical silica colloids with mean diameters of 80 nm and 590 nm by following the St \ddot{O} ber process.[35] After completely removing unreacted chemicals in three centrifugation/redispersion cycles, the purified silica colloids are well-dispersed in UV-curable

ethoxylated trimethylolpropane triacrylate (ETPTA) monomers (SR 454, Sartomer) with 1 vol% of 2-hydroxy-2-methyl-1-phenyl-1-propanone (Darocur 1173, BASF) as a photo-initiator using an ultrasonic homogenizer (Qsonica Sonicator Q700, Thermo Fisher Scientific). The silica colloid volume fraction is controlled to be 15 vol%. Owing to the electrostatic repulsion forces between silica colloids (zeta potential of approximately -42 mV), the colloidal suspension can be electrically stabilized for weeks.[36–38].

Self-Assembly of Double-Monolayer Silica Colloidal Crystals with Non-Close-Packed Arrangements. After filtration through a syringe filter (Millex-SV 5.0 μ m, Merck KGaA) to eliminate any colloid aggregate, the as-prepared 80 nm silica colloidal suspension is deposited and spread on a commercial poly(ethylene terephthalate) (PET) film (1.0 mm in thickness, Wisegate Technology), which is rinsed with anhydrous ethanol before use. The PET substrate is then spun at 2500 rpm for 30 s, 5000 rpm for 30 s, and 7500 rpm for 240 s to remove excess suspension using a spin-processor (WS-650-23B, Laurell), during which a non-close-packed 80 nm silica colloidal monolayer is self-assembled. The ETPTA monomers can be photo-polymerized by exposure to ultraviolet radiation for 5 s (X LiteTM 500, OPAS). Subsequently, a uniform poly(ETPTA) film is spin-coated onto the 80 nm silica colloidal crystals at a spin speed of 5000 rpm for 60 s. Afterwards, non-close-packed monolayer 590 nm silica colloidal crystals are self-assembled at 2500 rpm for 30 s, 5000 rpm for 30 s, and 7500 rpm for 45 s onto the poly(ETPTA) film, followed by a photo-polymerization process.

Templating Fabrication of Termite-Wing-Inspired Hierarchical Structure Arrays. The double-monolayer silica colloidal crystals are utilized as etching masks to pattern hierarchical structure arrays in an inductively coupled plasma-reactive ion etcher (Unaxis Shuttlelock 700 series, OC Oerlikon) for 20 min. During the reactive ion etching (RIE) process, oxygen/argon flow rates are varied from 15/10 to 30/10 sccms under a constant chamber pressure (20 mTorr) and a fixed power density (50 W). After the colloidal lithography, the remained silica structural templates are wet-etched in a hydrofluoric acid aqueous solution (2 vol %), followed by rinsing with anhydrous ethanol.

Surface Modification of Hierarchical Structure Arrays. The surface of hierarchical structures is chemically functionalized with fluoride through a chemical vapor deposition process to improve its surface hydrophobicity. In the surface modification process, the structure-covered PET substrate is placed in a vacuum drying oven, on the bottom of which is dispensed a beaker of 1H,1H,2H,2H-heptadecafluorodecyl acrylate (97 vol%, Merck KGaA). Once pulling a vacuum on the oven that is maintained at 70 °C, the vaporized fluoride can react with the acrylate groups on the hierarchical structures below its regular boiling point.[39] After one and a half hours, the PET substrate is transferred to a vacuum chamber to evaporate any unreacted fluoride molecules remaining on the substrate.

Characterization. Photographic images and surface morphologies of the specimens are acquired from a digital camera (NIKKOR Z, Nikon) and a field-emission scanning electron microscope (JSM-63335F, JEOL). Thin platinum layers are sputter-deposited on the specimens prior to imaging the surface morphologies (Cressington 108, Ted Pella). Water contact angles of the specimens are carried out on a drop shape analyzer system (DSA100, KRÜSS). Using an automated liquid handling system, deionized water droplets (10 μ L) are pipetted onto the specimens before taking images. Based on B-spline snakes (active contours), DropSnake drop analysis software can automatically fit and shape the water drop profiles to determine water contact angles. In this study, the average of 10 water contact angles in different regions of each specimen is reported. Anti-fogging characterization of the specimens takes place in an artificial fogging testing chamber, in which an ultrasonic humidifier (HI3013, LAICA) is applied to regulate the relative humidity. The horizontally placed specimens are exposed to the foggy atmosphere for 3 min, and then tilted at 5° to the platform.

3. Results and discussion

Many terrestrial insects lose flight capacities in rain and even become victims of immobilization on wetted surfaces. Formosan subterranean termites are with a high ratio of wing surface area to body volume (Fig. 1 (a)), which implies that they are more susceptible to water. Instead of thick and rigid cuticles, the termites utilize hydrophobic materials and topographic structuring to achieve water-resistant wings. It is found that micrometer-scale hairs, with an average height of 30 μm and an average base diameter of 590 nm, are evenly spaced on the wing membrane surface (Fig. 1 (b)-(c)). The micrometer-scale conical structures greatly reduce the contact area between bulk water and the wing. Interestingly, the hairs are surrounded by randomly arranged nanometer-scale waxy patches (Fig. 1 (d)). The wax protuberances are with ~ 80 nm in size, which play an important role in anti-fogging performance. As displayed in Fig. 2 (a) and (b), the water droplet exhibits a remarkable static water contact angle of 172.3° with the underlying termite wing. The suspension of water droplet indicates that the wing is with an inherent ability to repel and prevent water from spreading out. Besides that, the advancing water contact angle (174.2°) and the receding water contact angle (171.6°) of Formosan subterranean termite wing during wetting/dewetting processes are fairly similar to each other (Fig. 2 (c) and (d)). The results further suggest that the wing allows water droplets and any water-based debris collected on the surface to be removed easily at low sliding angles, commonly by gravity. Apparently, the micrometer-scale hairs exhibit superhydrophobic characteristics, and function as an ultra-low adhesion barrier to water. It is worth mentioning that the combination of hairs and wax patches can even act as an anti-fogging coating. To evaluate their anti-fogging behaviors, a horizontally placed termite wing with a cover glass underneath is exposed to an artificial fog-filled environment for 3 min, and then tilted at an angle of 5° . By comparing the photographic images of the specimen before and after exposure to fog (Fig. 2 (e) and (f)), it is evident that fogs condense, grow, and adhere onto the glass reference, leading to a hazy appearance. In sharp contrast to that, almost no fog is stuck on the Formosan subterranean termite wing, while the characters beneath it are clearly observed. It indicates that the hierarchical structures are designed to minimize the solid/water contact area, and to reduce the interaction

with water droplets of various size scales (Figure S1).[40,41] The resulting negligible adhesion allows water microdroplets to roll and merge with each other by minor movements/vibrations of the wing. Consistent wetting therefore makes microdroplets keep building up in size until they are large enough for removal by large droplets resting on the hairs. The termite wing can then be anchored at one end to shed the accumulated fog droplets off its surface.

Inspired by the anti-wetting characteristics of Formosan subterranean termite wings, hierarchical structure arrays are engineered through integrating a shear-induced colloidal self-assembly technology and a colloidal lithography nanofabrication strategy. As illustrated in the experimental scheme (Fig. 3), a monolayer of 80 nm silica colloid/poly(ETPTA) composite is spin-coated on a PET substrate. In the spin-coating process, the 80 nm silica colloids are shear-aligned into a hexagonal non-close-packed arrangement. After coating a uniform poly(ETPTA) layer, another monolayer of non-close-packed 590 nm silica colloid/poly(ETPTA) composite is spin-coated onto the substrate. Owing to a high etching selectivity between silica and polymers using oxygen and argon plasma, the double-monolayer silica colloidal crystals serve as etching masks to preserve the polymers underneath them during the RIE process.[42] It is worthy to note that the size and aspect ratio of the as-patterned polymeric structure can be controlled through adjusting silica colloid size and tuning RIE parameters. Afterwards, the silica tops are wet-etched by hydrofluoric acid to engineer Formosan subterranean termite-inspired hierarchical structure arrays.

The two-dimensional orderings of the spin-coated silica colloids are displayed in Fig. 4 (a)-(d). Even though a few defects and misaligned lines, mostly caused by dust particles with distinct sizes, are noticed, not only 80 nm silica colloids but also 590 nm silica colloids are self-assembled into hexagonal non-close-packed arrangements. In addition, their average inter-colloid distances equal to approximate $\sqrt{2} D$, in which D refers to the silica colloid diameter. It is worthy to mention that visible light diffraction on the spin-coated silica colloidal crystals leads to a characteristic six-arm pattern (Fig. 4 (e)), which is identical to that of hexagonal non-close-packed structures.[43] This photographic image further discloses that the periodic domain over a centimeter-scale is achieved. Importantly, it is evident that a poly(ETPTA) film ($\sim 2 \mu\text{m}$ in thickness) is sandwiched between the double-monolayer silica colloidal

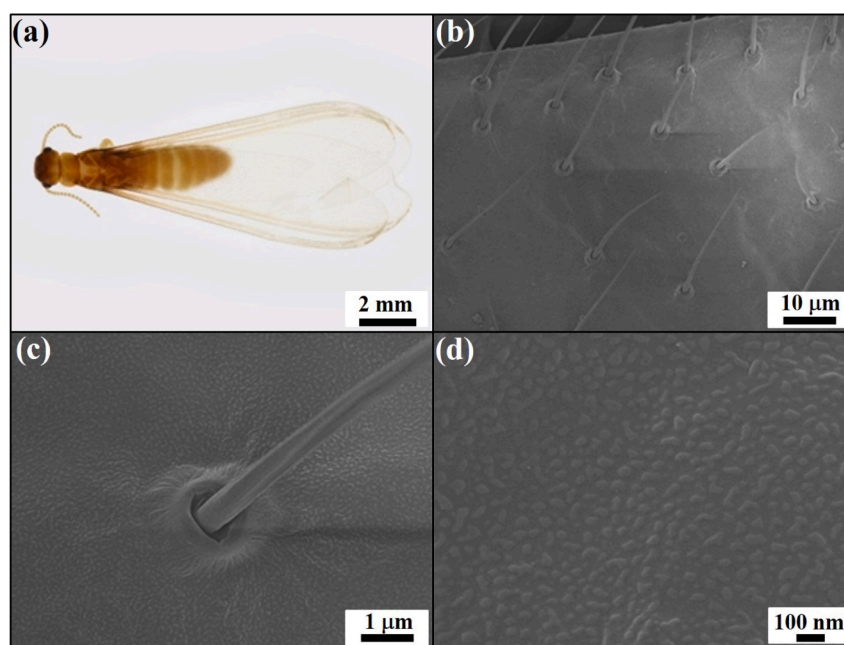


Fig. 1. Ultrastructure of the Formosan subterranean termite wing. (a) Photographic image of a winged Formosan subterranean termite taken under natural light illumination from dorsal view. (b) SEM image of the wing showing micrometer-scale conical structures, hairs, evenly spaced on the wing membrane surface. (c) Magnified SEM image of the hair and the hair socket. (d) Higher resolution SEM image showing the wing surface covered with nanometer-scale wax patches.

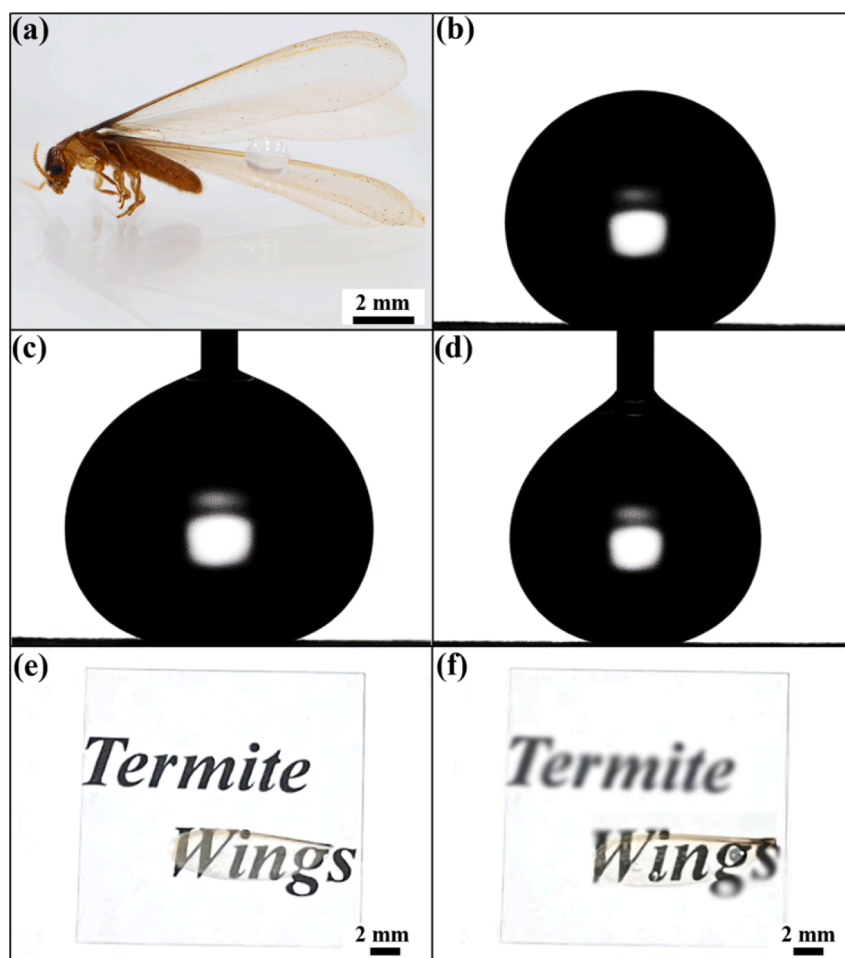


Fig. 2. Anti-wetting and anti-fogging characteristics of the Formosan subterranean termite wings. (a) Lateral view of a winged termite showing suspension of a water droplet above the wing membrane. (b) Static water contact angle, (c) advancing water contact angle, and (d) receding water contact angle on the wing. Photographic images of a termite wing placed on a 2x2 cm cover glass (e) before and (f) after exposure to fog in a fogging testing chamber.

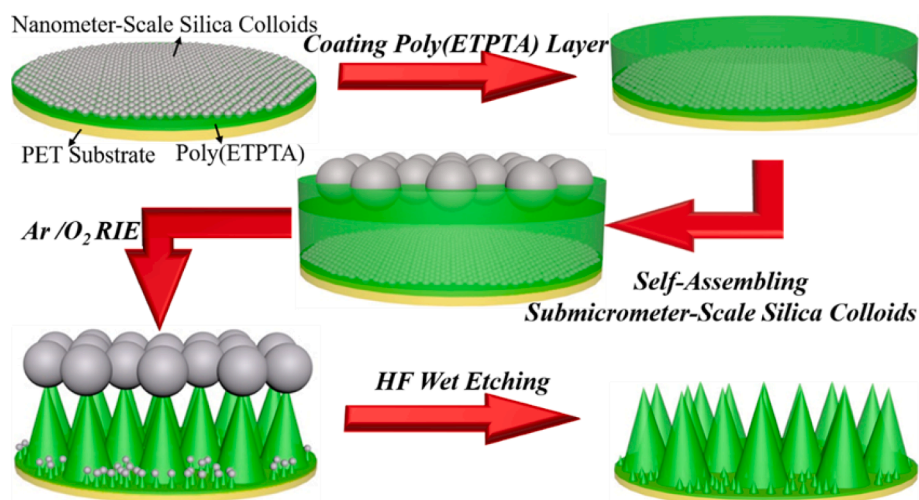


Fig. 3. Schematic illustration of fabrication procedures for engineering Formosan subterranean termite-inspired hierarchical structure arrays.

crystals (Fig. 4 (f)). The film thickness from micrometer-scale to nanometer-scale is controllable through spin-coating at a variable speed. [44].

The polymer constituent of the double-monolayer silica colloidal crystal-coated PET film is selectively plasma-etched by concurrent

oxygen and argon reactive ions, during which the silica colloidal crystals are employed as etching masks to shield the polymers beneath. In the etching process, the oxygen/argon flow rates are fixed at 15/10 sccms. It is found that the hexagonal non-close-packed arrangements of 590 nm and 80 nm silica colloidal crystals are well-preserved, while the

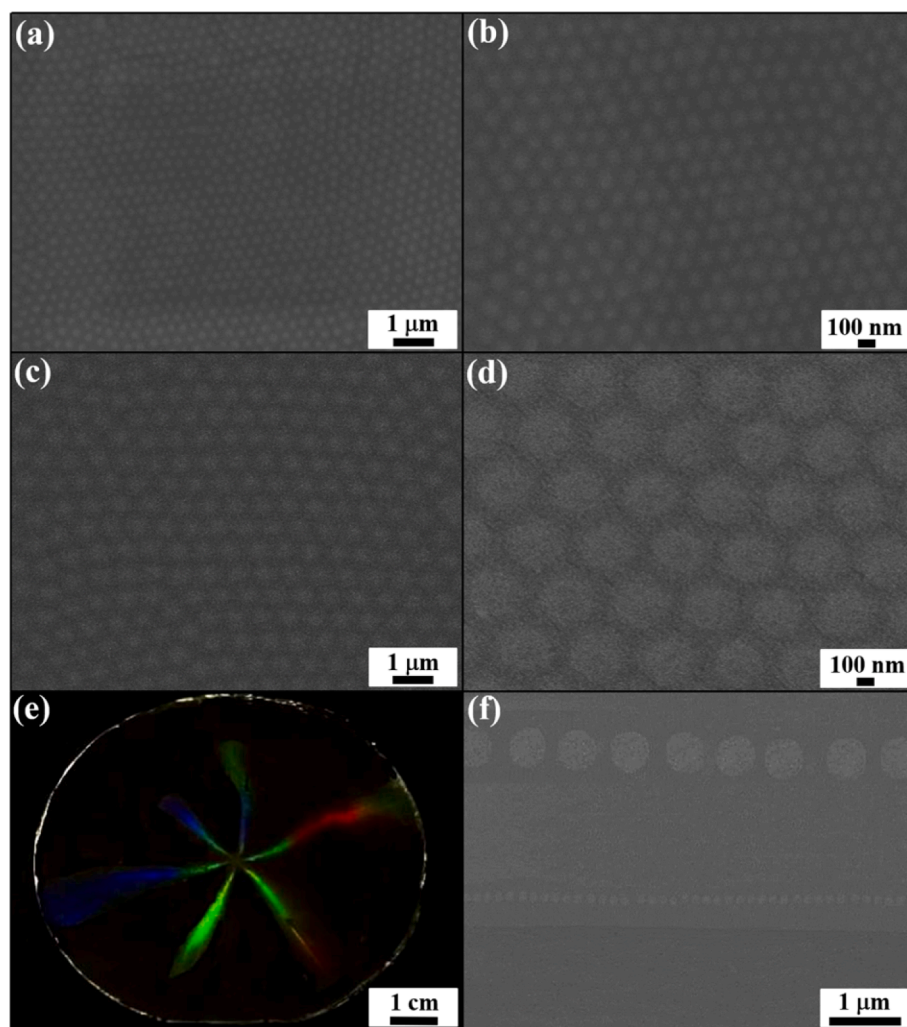


Fig. 4. (a) Top-view SEM image of non-close-packed monolayer 80 nm silica colloidal crystals spin-coated on a PET substrate. (b) Magnified top-view SEM image of (a). (c) Top-view SEM image of non-close-packed monolayer 590 nm silica colloidal crystals spin-coated on the 80 nm silica colloidal crystals. (d) Magnified top-view SEM image of (c). (e) Photographic image of the double-monolayer silica colloidal crystal-coated PET substrate. (f) Side-view SEM image of the double-monolayer silica colloidal crystals.

shrinkage of silica colloids is not significant in the RIE process (Fig. 5 (a) and (b)). The combination of isotropic etching and anisotropic etching leads to the formation of chess-pawn-like features, comprising of conical polymer bottoms and spherical silica tops (Fig. 5 (c) and (d)). As a result, periodically arranged micrometer-scale chess-pawn-like structures are surrounded by nanometer-scale chess-pawn-like structures. The templating silica tops are then selectively wet-etched to engineer hierarchical conical structure arrays (Fig. 5 (e) and (f)). It appears that the structures can maintain their inter-particle distance and long-range ordering throughout the templating process. Nevertheless, the anti-wetting performance of the as-engineered structure arrays is not comparable with that of termite wings (Figure S2).

Formosan subterranean termite wings, primarily made of chitin fibers, are covered by micrometer-scale wax-covered hairs and nanometer-scale wax patches.[45] The low surface energy material-covered hierarchical structures can function as a waterproofing barrier on the wing membrane surface to improve its flight capability in rain as well as in foggy conditions. Taking a lesson from the termite, the surface hydrophobicity of the as-engineered hierarchical conical structure arrays is ameliorated through surface functionalizing with 1H,1H,2H,2H-heptadecafluorodecyl acrylate. The suspension of spherical water droplets, with an average static water contact angle of 175.3° , above the surface-modified structure-coated substrate is observed (Fig. 6 (a) and (b)). The non-wetting water droplets tend to roll off the substrate and carry contaminating particles away at a low water contact angle hysteresis, referring to a small difference between the advancing water

contact angle (177.3°) and the receding water contact angle (174.6°) (Fig. 6 (c) and (d)). To further assess its anti-fogging capability, photographic images of the specimen with a glass substrate underneath before and after exposure to fog are presented (Fig. 6 (e) and (f)). Apparently, either one possesses a high optical transparency, and almost no fog droplets remain on the surface. Owing to the low surface energy and small water/solid contact area, the adhesion of fog droplets with different sizes is minimized on the hierarchical conical structure arrays (Fig. 7). On that account, fog microdroplets migrate effortlessly and merge into larger ones during the fog droplet growth process. The fog droplets resting on the nanometer-scale conical structures can be absorbed by large droplets held above the micrometer-scale conical structures, and then slide off at a small tilting angle. In comparison with the wetting behaviors of a surface-modified bare substrate (Figure S3), it is evident that the self-cleaning and anti-fogging characteristics are improved by introducing the hierarchical conical structure arrays. Crucially, the presence of micrometer-scale conical structures can only bring about superhydrophobic and self-cleaning surfaces, but can't resist the condensation and adherence of fog microdroplets between the structures (Figure S4). On the other hand, neither anti-wetting nor anti-fogging performance can be apparently improved on the nanometer-scale conical structure-covered substrate (Figure S5).

To further comprehend the dependence of structure configuration on anti-wetting capabilities, hierarchical inclined conical structures are engineering through tuning oxygen flow rate from 15 to 30 sccm (Figure S6). As mentioned previously, the highly ordered double-

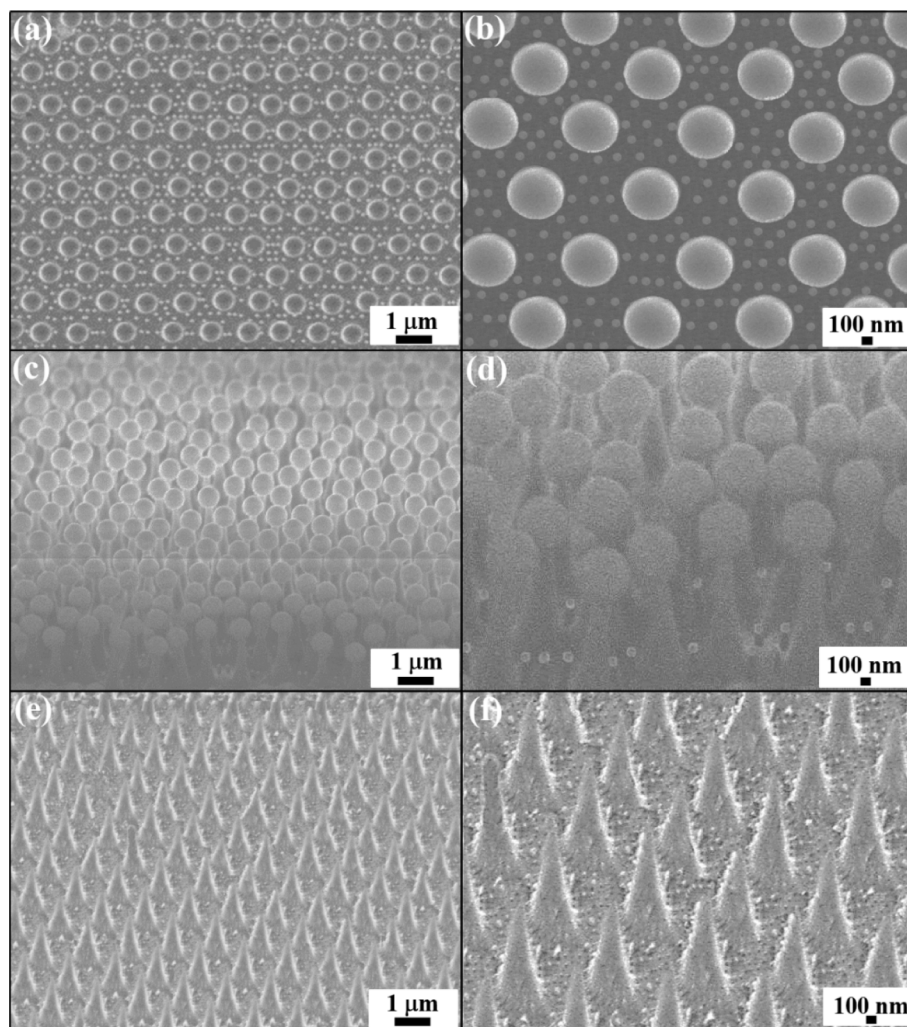


Fig. 5. (a) Top-view SEM image of hierarchical chess-pawn-like structure arrays templated from the double-monolayer silica colloidal crystals by reactive ion etching. (O_2 (15 SCCM)/Ar (10 SCCM)) (b) Magnified top-view SEM image of (a). (c) Tilted-view SEM image of (a). (d) Magnified tilted-view SEM image of (c). (e) Tilted-view SEM image of hierarchical conical structure arrays templated from the double-monolayer silica colloidal crystals. (f) Magnified tilted-view SEM image of (e).

monolayer silica colloidal crystals can be retained and serve as etching masks during the oxygen and argon RIE process (Figure S7 (a) and (b)). The increase of isotropic oxygen RIE leads to the formation of polymeric conical structures with slender and sharp tips (Figure S7 (c) and (d)). Interestingly, the tips are too fragile to fully support the above structural templates, and hence the chess-pawn-like structures automatically bend in random directions. It is worth noting that the non-close-packed arrangement of structure arrays renders adequate inter-structural space to develop inclined structures. After wet-etching the silica templates, hierarchical inclined conical structure arrays are directly patterned on the substrate (Figure S7 (e) and (f)). Compared with the structure configuration of nanometer-scale conical structures, it is found that the micrometer-scale conical structures are highly inclined and with even sharper tips, resulting from the exposure of longer RIE. Although the tips of micrometer-scale conical structures are in contact with each other, attributed to the van der Waals forces among neighboring structures, the inclined structures are not intensely bunched to form large-area collapsed bundles.

After surface modification with fluoride, water droplets with an average contact angle of 153.4° are performed on the hierarchical inclined conical structure-coated substrate (Figure S8 (a) and (b)). Even if a superhydrophobic state is achieved, the corresponding surface hydrophobicity is significantly decreased in comparison with that of

surface-modified hierarchical conical structure-coated substrate. The wetting behaviors on structured substrates can be expounded using the Cassie-Baxter equation, $\cos\theta_c = f\cos\theta - (1-f)$, in which θ_c and θ denote the static water contact angles on structure-coated substrates and bare substrates, respectively, while f represents the fraction of the projected area that is in direct contact with a water droplet out of the whole projected area. [46] For stronger isotropic RIE treatments, the formation of inclined structures generates larger wetted contact area fractions (f), and hence brings about lower static water contact angles (θ_c). The decrease in surface hydrophobicity leads to a distinguishable difference between the advancing water contact angle (158.3°) and the receding water contact angle (149.7°) (Figure S8 (c) and (d)), indicating that water droplets can adhere to the substrate until a tilting angle larger than 8.6° is applied. According to that, water microdroplets are able to anchor and grow in size on the hierarchical inclined conical structures under foggy conditions. As a result, fog droplets with varied sizes are formed and remain on the substrate, leading to a hazy appearance and blurred characters underneath on exposure to fog (Figure S8 (e) and (f)). It further indicates that the air trapped between the micrometer-scale inclined conical structures prevents water droplets above them from contacting the water microdroplets resting on the nanometer-scale structures (Figure S9). It is apparent that not only a high surface hydrophobicity, but self-cleaning properties as well are required to realize

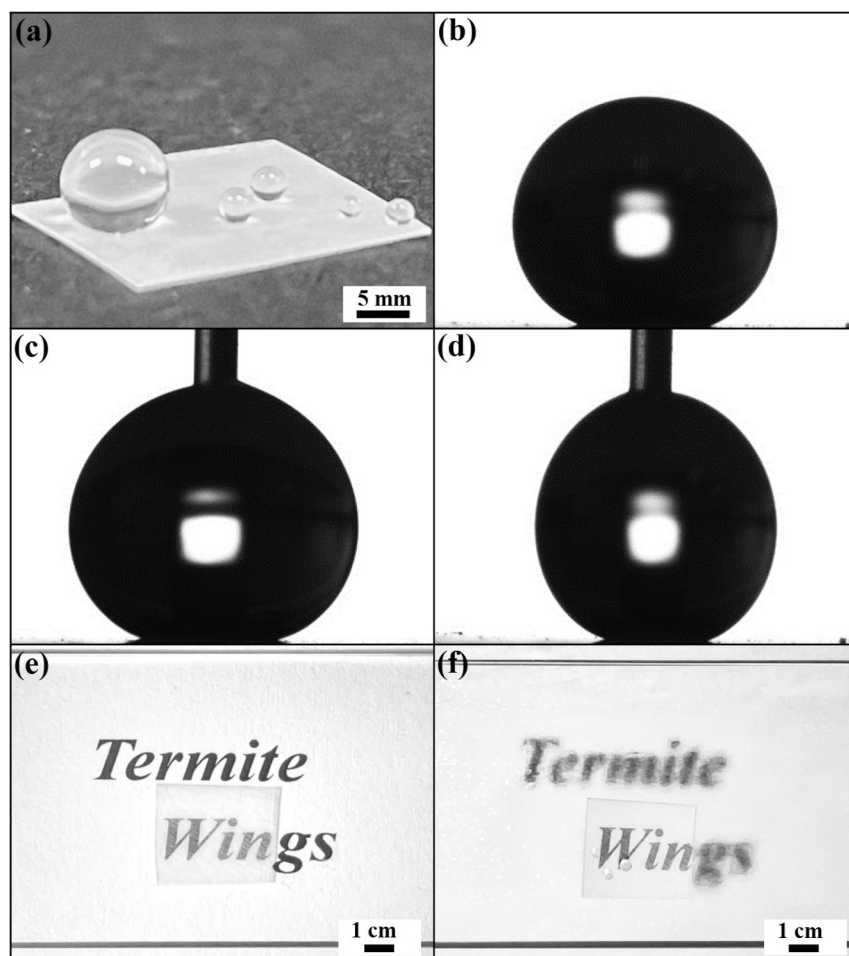


Fig. 6. Wetting characteristics of the hierarchical conical structure arrays templated from the double-monolayer silica colloidal crystals by reactive ion etching. (O_2 (15 SCCM)/Ar (10 SCCM)). (a) Photographic image showing suspension of water droplets above the hierarchical conical structure-coated PET substrate. (b) Static water contact angle, (c) advancing water contact angle, and (d) receding water contact angle on the PET substrate. Photographic images of the hierarchical conical structure-coated PET substrate placed on a glass slide (e) before and (f) after exposure to fog in a fogging testing chamber.

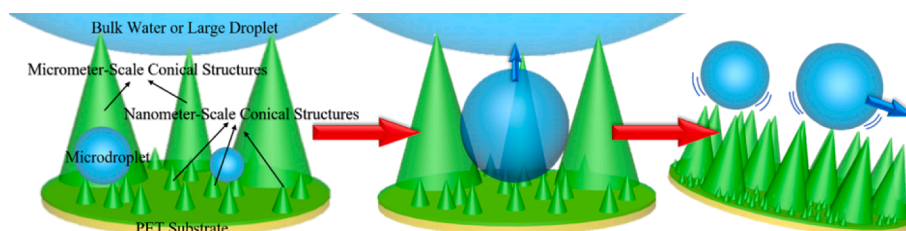


Fig. 7. Diagrammatic representation of the hierarchical conical structure arrays engineered to minimize interaction with water bodies with various sizes.

the anti-fogging functionality. Further experiments are in progress toward optimal anti-fogging structures.

4. Conclusions

In summary, double-monolayer non-close-packed silica colloidal crystals are self-assembled to serve as structural templates for engineering superhydrophobic hierarchical conical structure arrays, which inspired by Formosan subterranean termite wings. The integration of micrometer-scale and nanometer-scale conical structure arrays demonstrates an elegant design to minimize interaction with water droplets of various size scales. Fog microdroplets resting on the nanometer-scale structures can be absorbed by large ones held above the micrometer-scale structures, and then roll off at a small tilting angle of 2.7° . In comparison with the wetting behaviors of micrometer-scale structure array and hierarchical inclined conical structure arrays, the hierarchical conical structure arrays exhibit superior self-cleaning and anti-fogging

capabilities, even better than termite wings (Table 1). It appears that the Formosan subterranean termite-inspired anti-wetting structures will ultimately contribute to the next generation of multifunctional materials and lab-on-a-chip devices.

CRediT authorship contribution statement

Chung-Jui Lai: Conceptualization, Data curation, Methodology, Writing – original draft. **You-Jie Chen:** Formal analysis, Writing – original draft. **Mei-Xuan Wu:** Writing – original draft. **Chia-Chien Wu:** Writing – original draft. **Nien-Ting Tang:** Writing – original draft. **Ting-Fang Hsu:** Writing – original draft. **Shin-Hua Lin:** Writing – original draft. **Hou-Feng Li:** Conceptualization, Writing – review & editing, Supervision, Project administration, Funding acquisition. **Hongta Yang:** Conceptualization, Writing – review & editing, Supervision, Project administration, Funding acquisition.

Table 1

Static water contact angles, advancing water contact angles, receding water contact angles, water contact angle hystereses, sliding angles, and anti-fogging characteristics of a hierarchical conical structure-coated substrate, a micrometer-scale conical structure-coated substrate, a Formosan subterranean termite wing, a hierarchical inclined conical structure-coated substrate, a nanometer-scale conical structure-coated substrate, and a bare substrate. For each measurement, means followed by the same capital letter within a column are not significantly different at the $\alpha = 0.05$ level ($n = 9$, ANOVA followed by HSD test; PAST software, version 3.14). [47].

| | Static W.C.A. | Advancing W.C.A. | Receding W.C.A. | W.C.A. Hysteresis | Sliding Angle | Anti-Fogging |
|---|----------------|------------------|-----------------|-------------------|---------------|--------------|
|  | 175.3° ± 2° A | 177.3° ± 1° A | 174.6° ± 1° A | 2.7° ± 1° A | 2.2° ± 1° A | ○ |
|  | 174.9° ± 1° AB | 176.8° ± 2° A | 173.9° ± 1° A | 2.9° ± 1° A | 2.3° ± 1° A | × |
|  | 172.3° ± 4° B | 174.2° ± 3° B | 171.6° ± 3° B | 2.6° ± 3° A | 1.9° ± 3° A | ○ |
|  | 153.4° ± 3° C | 158.3° ± 2° C | 149.7° ± 3° C | 8.6° ± 2° B | 8.1° ± 2° B | × |
|  | 151.2° ± 1° C | 158.1° ± 3° C | 142.6° ± 1° D | 15.5° ± 1° C | 15.1° ± 1° C | × |
|  | 109.8° ± 1° D | 115.6° ± 1° D | 89.9° ± 1° E | 25.7° ± 1° D | 25.5° ± 1° D | × |

Declaration of Competing Interest

The authors declare that they have no known competing financial interests or personal relationships that could have appeared to influence the work reported in this paper.

Data availability

Data will be made available on request.

Acknowledgment

This research is financially supported by National Science and Technology Council, Taiwan (Grant MOST 110-2221-E-005-010, MOST 110-2221-E-005-050-MY2, and MOST 110-2628-B-005-001) and by the ENABLE Center, National Chung Hsing University. Acknowledgment is made to the Instrument Center of National Chung Hsing University for the use of Field Emission Scanning Electron Microscope.

Appendix A. Supplementary material

Supplementary data to this article can be found online at <https://doi.org/10.1016/j.apsusc.2023.156484>.

References

- M.J. Li, T.Z. Yang, Q. Yang, Z. Fang, H. Bian, C.J. Zhang, X. Hou, F. Chen, Bioinspired anti-fogging and anti-fouling artificial compound eyes, *Adv. Opt. Mater.* 10 (2022) 13.
- J. Tan, P.H. Tian, M.Y. Sun, H.C. Wang, N. Sun, G.J. Chen, Y.C. Song, D.Y. Jiang, H. Jiang, M.Y. Xu, A transparent electrowetting-on-dielectric device driven by triboelectric nanogenerator for extremely fast anti-fogging, *Nano Energy* 92 (2022) 9.
- Y. Li, W. Ma, Y.S. Kwon, W.H. Li, S.H. Yao, B.L. Huang, Solar deicing nanocoatings adaptive to overhead power lines, *Adv. Funct. Mater.* 32 (2022) 9.
- P. Ge, S.L. Wang, J.H. Zhang, B. Yang, Micro-/nanostructures meet anisotropic wetting: from preparation methods to applications, *Mater. Horizons* 7 (2020) 2566–2595.
- X. Yan, Z.Y. Huang, S. Sett, J. Oh, H. Cha, L.N. Li, L.Z. Feng, Y.F. Wu, C.Y. Zhao, D. Orejon, F. Chen, N. Miljkovic, Atmosphere-mediated superhydrophobicity of rationally designed micro/nanostructured surfaces, *ACS Nano* 13 (2019) 4160–4173.
- Q. Yang, Z.W. Zhu, S. Tan, Y.M. Luo, Z.Z. Luo, How micro-/nanostructure evolution influences dynamic wetting and natural deicing abilities of bionic lotus surfaces, *Langmuir* 36 (2020) 4005–4014.
- Y.X. Zuo, L.Z. Zheng, C. Zhao, H. Liu, Micro-/nanostructured interface for liquid manipulation and its applications, *Small* 16 (2020) 29.
- M.Q. Hovish, F. Hilt, N. Rolston, R. Xiao, R.H. Dauskardt, Open air plasma deposition of superhydrophilic titania coatings, *Adv. Funct. Mater.* 29 (2019) 9.
- Y.J. Cao, A. Salvini, M. Camaiti, One-step fabrication of robust and durable superamphiphobic, self-cleaning surface for outdoor and in situ application on building substrates, *J. Colloid Interface Sci.* 591 (2021) 239–252.
- X.B. Wang, J.X. Huang, Z.G. Guo, Overview of the development of slippery surfaces: Lubricants from presence to absence, *Adv. Colloid Interface Sci.* 301 (2022) 25.
- Y.X. Chen, K. Li, S.D. Zhang, L. Qin, S.H. Deng, L.Y. Ge, L.P. Xu, L.L. Ma, S.T. Wang, X.J. Zhang, Bioinspired superwetable microspine chips with directional droplet transportation for biosensing, *ACS Nano* 14 (2020) 4654–4661.
- F. Geyer, M. D'Acunzi, A. Sharifi-Aghili, A. Saal, N. Gao, A. Kaltbeitzel, T.F. Sloat, R. Berger, H.J. Butt, D. Vollmer, When and how self-cleaning of superhydrophobic surfaces works, *Sci. Adv.* 6 (2020) 11.
- J.Y. Long, P.X. Fan, D.W. Gong, D.F. Jiang, H.J. Zhang, L. Li, M.L. Zhong, Superhydrophobic surfaces fabricated by femtosecond laser with tunable water adhesion: from lotus leaf to rose petal, *ACS Appl. Mater. Interfaces* 7 (2015) 9858–9865.
- W.L. Min, B. Jiang, P. Jiang, Bioinspired self-cleaning antireflection coatings, *Adv. Mater.* 20 (2008) 3914.
- X. Xiao, C.H. Zhang, H.Y. Ma, Y.H. Zhang, G.L. Liu, M.Y. Cao, C.M. Yu, L. Jiang, Bioinspired slippery cone for controllable manipulation of gas bubbles in low-surface-tension environment, *ACS Nano* 13 (2019) 4083–4090.
- W.W. Ding, C.A. Dorao, M. Fernandez, Improving superamphiphobicity by mimicking tree-branch topography, *J. Colloid Interface Sci.* 611 (2022) 118–128.
- X.M. Feng, H.Y. Guan, Z. Wang, S.C. Niu, Z.W. Han, Biomimetic slippery PDMS film with papillae-like microstructures for antifogging and self-cleaning, *Coatings* 11 (2021) 13.
- R. Nishimura, K. Hyodo, H. Mayama, S. Yokojima, S. Nakamura, K. Uchida, Dual wettability on diarylethene microcrystalline surface mimicking a termite wing, *Comm. Chem.* 2 (2019) 11.
- A.J. Blumenfeld, P.A. Eyer, C. Husseneder, J.C. Mo, L.N.L. Johnson, C.L. Wang, J. K. Grace, T. Chouvenec, S.C. Wang, E.L. Vargo, Bridgehead effect and multiple introductions shape the global invasion history of a termite, *Commun. Biol.* 4 (2021) 12.
- X. Deng, L. Mammen, H.J. Butt, D. Vollmer, Candle soot as a template for a transparent robust superamphiphobic coating, *Science* 335 (2012) 67–70.
- M. Asghari, X.B. Cao, B. Mateescu, D. van Leeuwen, M.K. Aslan, S. Stavarakis, A. J. Demello, Oscillatory viscoelastic microfluidics for efficient focusing and separation of nanoscale species, *ACS Nano* 14 (2020) 422–433.
- C.L. Chen, D. Weng, A. Mahmood, S. Chen, J.D. Wang, Separation mechanism and construction of surfaces with special wettability for oil/water separation, *ACS Appl. Mater. Interfaces* 11 (2019) 11006–11027.

- [23] W.S. Deng, G. Wang, L. Tang, Z.X. Zeng, T.H. Ren, One-step fabrication of transparent Barite colloid with dual superhydrophilicity for anti-crude oil fouling and anti-fogging, *J. Colloid Interface Sci.* 608 (2022) 186–192.
- [24] I.R. Duran, G. Laroche, Water drop-surface interactions as the basis for the design of anti-fogging surfaces: Theory, practice, and applications trends, *Adv. Colloid Interface Sci.* 263 (2019) 68–94.
- [25] P. Gao, Y.L. Wang, J. Wang, F.S. Wang, W. Ma, Z.Z. Zhang, X.H. Men, Y. Lu, Rational design of durable anti-fouling coatings with high transparency, hardness, and flexibility, *ACS Appl. Mater. Interfaces* 14 (2022) 29156–29166.
- [26] W. Huang, J.X. Huang, Z.G. Guo, W.M. Liu, Icephobic/anti-icing properties of superhydrophobic surfaces, *Adv. Colloid Interface Sci.* 304 (2022) 30.
- [27] G.H. Zhang, Y. Liu, C. Chen, C.Y. Huang, L.L. Long, S.R. Zhang, G. Yang, F. Shen, X. H. Zhang, Y.Z. Zhang, Green, robust self-cleaning superhydrophilic coating and on-demand oil-water separation, *Appl. Surf. Sci.* 595 (2022) 10.
- [28] Q.B. Dong, F.L. Zhou, J. Jiang, W.W.L. Xu, D. Behera, B. Sengupta, M. Yu, Advanced functional hierarchical nanoporous structures with tunable microporous coatings formed via an interfacial reaction processing, *ACS Appl. Mater. Interfaces* 12 (2020) 26360–26366.
- [29] W.F. Liu, J.B. Wang, X.Z. Xu, C.Z. Zhao, X.B. Xu, P.S. Weiss, Single-step dual-layer photolithography for tunable and scalable nanopatterning, *ACS Nano* 15 (2021) 12180–12188.
- [30] Z.C. Fan, M. Grunwald, Orientational order in self-assembled nanocrystal superlattices, *J. Am. Chem. Soc.* 141 (2019) 1980–1988.
- [31] V.S. Vendamani, S. Rao, A.P. Pathak, V.R. Soma, Silicon nanostructures for molecular sensing: a review, *ACS Appl. Nano Mater.* 5 (2022) 4550–4582.
- [32] J.Y. Chen, L.H. Yuan, C. Shi, C.Q. Wu, Z.W. Long, H. Qiao, K.L. Wang, Q.H. Fan, Nature-inspired hierarchical protrusion structure construction for washable and wear-resistant superhydrophobic textiles with self-cleaning ability, *ACS Appl. Mater. Interfaces* 13 (2021) 18142–18151.
- [33] H.B. Wang, W. Chen, B. Chen, Y. Jiao, Y. Wang, X.P. Wang, X.C. Du, Y. Hu, X.X. Lv, Y.S. Zeng, X.F. Wang, L.M. Qian, J. Xiong, Interfacial capillary-force-driven self-assembly of monolayer colloidal crystals for supersensitive plasmonic sensors, *Small* 16 (2020) 9.
- [34] M. Khan, A. Hamid, T.H. Li, A. Zada, F. Attique, N. Ahmad, A. Ullah, A. Hayat, I. Mahmood, A. Hussain, Y. Khan, I. Ahmad, A. Ali, T.K. Zhao, Surface optimization of detonation nanodiamonds for the enhanced mechanical properties of polymer/nanodiamond composites, *Diam. Relat. Mat.* 107 (2020) 9.
- [35] W. Stöber, A. Fink, E. Bohn, Controlled growth of monodisperse silica spheres in the micron size range, *J. Colloid Interface Sci.* 26 (1968) 62–69.
- [36] W.L. Min, P. Jiang, B. Jiang, Large-scale assembly of colloidal nanoparticles and fabrication of periodic subwavelength structures, *Nanotechnology* 19 (2008) 7.
- [37] C.H. Sun, P. Jiang, B. Jiang, Broadband moth-eye antireflection coatings on silicon, *Appl. Phys. Lett.* 92 (2008) 3.
- [38] M. Khan, L. Tiehu, A. Hussain, A. Raza, A. Zada, D. Alei, A.R. Khan, R. Ali, H. Hussain, J. Hussain, Z. Wahab, M. Imran, Physicochemical evaluations, mechanical attenuations and thermal stability of graphene nanosheets and functionalized nanodiamonds loaded pitch derived carbon foam composites, *Diam. Relat. Mat.* 126 (2022) 11.
- [39] I. Junkar, M. Modic, M. Mozeti, Modification of PET surface properties using extremely non-equilibrium oxygen plasma, *Open Chem.* 13 (2015) 490–496.
- [40] G.S. Watson, B.W. Cribb, J.A. Watson, How micro/nanoarchitecture facilitates anti-wetting: an elegant hierarchical design on the termite wing, *ACS Nano* 4 (2010) 129–136.
- [41] G.S. Watson, B.W. Cribb, J.A. Watson, Contrasting micro/nano architecture on termite wings: two divergent strategies for optimising success of colonisation flights, *PLoS One* 6 (2011) 10.
- [42] J.B. Kim, S.Y. Lee, J.M. Lee, S.H. Kim, Designing structural-color patterns composed of colloidal arrays, *ACS Appl. Mater. Interfaces* 11 (2019) 14485–14509.
- [43] Y.J. Zhao, L.R. Shang, Y. Cheng, Z.Z. Gu, Spherical colloidal photonic crystals, *Accounts Chem. Res.* 47 (2014) 3632–3642.
- [44] G.S. Watson, J.A. Watson, Natural nano-structures on insects - possible functions of ordered arrays characterized by atomic force microscopy, *Appl. Surf. Sci.* 235 (2004) 139–144.
- [45] M.A. Sani, M. Maleki, H. Eghbaljoo-Gharehgheshlaghi, A. Khezerlou, E. Mohammadian, Q. Liu, S.M. Jafari, Titanium dioxide nanoparticles as multifunctional surface-active materials for smart/active nanocomposite packaging films, *Adv. Colloid Interface Sci.* 300 (2022) 15.
- [46] S.D. Hong, M.Y. Ha, S. Balachandar, Static and dynamic contact angles of water droplet on a solid surface using molecular dynamics simulation, *J. Colloid Interface Sci.* 339 (2009) 187–195.
- [47] Ø. Hammer, D.A.T. Harper, P.D. Ryan, PAST: paleontological statistics software package for education and data analysis, *Palaeontol. Electron.* 4 (2001) 9.